Sister Rod Destructive Examinations (FY21)

Appendix G: CIRFT Uncertainty Calculations

Spent Fuel and Waste Disposition

SUMMARY

This document discusses the uncertainty of measurements associated with the cyclic integrated reversible-bending fatigue tester (CIRFT) system and the resulting uncertainty in the acquired measurements and calculated information. The primary parameters measured during the CIRFT test include the deflection magnitude of the specimen, the load applied during bending, and the number of cycles to specimen gross failure. The associated primary calculated parameters are the bending radius/curvature and the bending moment. Secondary calculated parameters include specimen stress and strain amplitudes, as well as flexural rigidity. The uncertainty associated with the primary and secondary calculated parameters is investigated based on the known uncertainty in the measured parameters.

This page is intentionally blank

CONTENTS

This page is intentionally blank

LIST OF FIGURES

This page is intentionally blank

LIST OF TABLES

This page is intentionally left blank.

REVISION HISTORY

Date	Changes
3/14/2021	Initial release
3/31/2022	The document number and date were updated for inclusion in the M2 report.

This page is intentionally left blank.

ACRONYMS

ASME	American Society of Mechanical Engineers
BWR	boiling water reactor
CIRFT	cyclic integrated reversible-bending fatigue tester
DE	destructive examination
DOE	US Department of Energy
FEA	finite element analysis
FHT	full-length fuel rod heat treatment
GTRF	grid-to-rod fretting
HBU	high burnup
ID	inner diameter
LSTC	Livermore Software Technology Corporation
LVDT	linear variable differential transducer
LT	low tin
NDE	nondestructive examination
NE	Office of Nuclear Energy
NRC	US Nuclear Regulatory Commission
OD	outer diameter
ORNL	Oak Ridge National Laboratory
PWR	pressurized water reactor
SNF	spent nuclear fuel

This page is intentionally left blank.

G-1. Introduction

Appendix F provides a description of the CIRFT equipment, the measurements taken, and the basic data processing and extended information derived from those measurements.

This document discusses the uncertainty of measurements associated with the CIRFT system and the resulting uncertainty in the acquired measurements and calculated information. The primary parameters measured during the CIRFT test include the deflection magnitude of the specimen, the load applied during bending, and the number of cycles to specimen gross failure. The associated primary calculated parameters are the bending radius/curvature and bending moment. Secondary calculated parameters include specimen stress and strain amplitudes, as well as flexural rigidity. The uncertainty associated with the primary and secondary calculated parameters are investigated based on the known uncertainty in the measured parameters.

G-2. Instrumentation and Equipment that Influence Accuracy

The information on the CIRFT equipment and instrumentation are taken from references G-1 and G-2. Information on the uncertainties of the various instrumentation were provided by Wang (personal communication via email, 12/15/2020 through 1/24/2021).

The bending radius and curvature are calculated from measurements taken by three identical linear variable differential transformers (LVDTs, RDP Electrosense, Inc. [RDP]) spaced at 12 ± 0.05 mm. The RDP LVDTs have a 5 mm stroke with a sensitivity that is 77.35 mV/V/mm and a V-to-mm calibration uncertainty of 2.6 μm at the time of installation in the hot cell, as shown in Eq. (G-3). The uncertainty in the deflection measurements and the LVDT spacing directly influences the accuracy of the reported curvature and the downstream strain and flexural rigidity results.

The average bending moment, M, is calculated as the loading arm length (fixed at 101.60 ± 0.05 mm) multiplied by the force applied as measured by the load cell. The load is measured using a Honeywell load cell with a maximum capacity of 4,448 N and an uncertainty of 0.2% of the full scale, 8.9 N. Uncertainty in the loading arm length is fixed and small. Uncertainty in the load cell influences the calculated bending moment, as well as and the downstream stress and flexural rigidity calculations.

Uncertainties related to the specimen-to-specimen differences in spent nuclear fuel (SNF) (e.g., dog-bone fabrication tolerances, epoxy strength, epoxy layer thickness, SNF surface spalling, or incipient cracks) are considered minor and are not addressed in this discussion. Likewise, uncertainties related to the hot cell environment (e.g., temperature, air flow) are not considered in this discussion.

G-3. Uncertainty Calculations

The 2σ uncertainties associated with the measurements are estimated by using a sum of squares of the individual variations assuming independence of the variables (no cross correlations):

$$U_f = \left[\left(\frac{\partial f}{\partial x}\right)^2 U_x{}^2 + \left(\frac{\partial f}{\partial y}\right)^2 U_y{}^2 + \left(\frac{\partial f}{\partial z}\right)^2 U_z{}^2 + \cdots\right]^{1/2}. \tag{G-1}$$

Where

U_f is the 2σ uncertainty of the function $f(x,y,z,...)$

$U_x, U_y, and\ U_z$ are the 2σ uncertainties of the measured values x,y,z.

The derivatives are evaluated at the nominal measured values (effectivity a single term Taylor series expansion assuming small variations).

G-3.1 Cycles-to-Failure Uncertainty

The primary parameter observed during the CIRFT test is the number of cycles to failure. The failure point is detected by the machine as an abrupt change in load. The number of cycles from crack formation to gross failure is unknown but is expected to be small in comparison with the total number of cycles. As observed in at least two sister rod specimens, a crack in the specimen may form without resulting in gross failure of the rod, so there is some uncertainty in the cycles-to-failure measurement. However, because no data are available to support uncertainty quantification, no further analysis is provided in this document. Future tests could investigate this parameter further

G-3.2 Curvature Uncertainty

The curvature, K, is calculated by determining the physical coordinates described by the measured LVDT deflections d_1, d_2, and d_3, by sensor spacing, and by scribing them with a circle of radius R.

$$R = \sqrt{(x_o - d_2)^2 + y_0^2}, \tag{G-2}$$

where:

$$x_0 = \frac{-2m_a m_b h - m_a(d_2 + d_3) + m_b(d_1 + d_2)}{2(m_b - m_a)}, \tag{G-3}$$

$$y_0 = -\frac{1}{m_a}\left(x_0 - \frac{d_1 + d_2}{2}\right) - \frac{h}{2}, \text{ and} \tag{G-4}$$

$$m_a = \frac{h}{d_2 - d_1} \text{ and } m_b = \frac{h}{d_3 - d_2}, \tag{G-5}$$

and h is the sensor distance fixed at 12 mm. The curvature of the scribed circle is 1/R.

G-3.2.1 Uncertainty related to d_1, d_2, and d_3

The amplitude magnitudes reported by the LVDT for d_1, d_2, and d_3 during a typical test are ~0.05 to 0.08 mm, as illustrated in Fig. G-1 (right) from reference G-1. Because the sensor configuration is symmetric, d_1, and d_3 are expected to be about the same, and the center probe deflection, d_2, is typically ~0.01 mm higher or lower, depending on the direction of the bending. In addition to the calibration uncertainty associated with the linearity of the LVDT probe, there is also some noise in the LVDT signal, as shown in Fig. 1 (left). From Fig. 1, the variance of the LVDT reading is on the order of 0.004 mm and the range of the LVDT reading is 0.12 mm (0.06 to -0.06 mm).

The combined amplitude uncertainty for the LVDT measurements of d_1, d_2, and d_3 is therefore estimated as 0.004 mm + 2.6 μm = 6.6E-06 m.
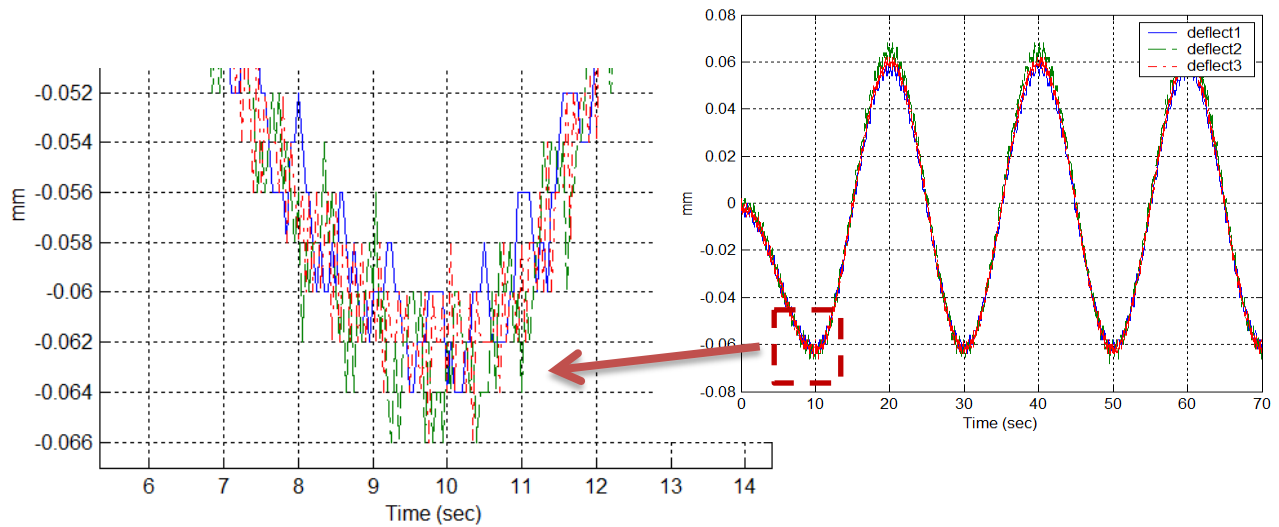
Figure G-1. Typical LVDT Output during CIRFT Test [G-1].

G-3.2.2 Uncertainty related to h

The initial uncertainty assigned to the nominal spacing of 12 mm is ± 0.05 mm.

It is also known that the flat head of the LVDT produces an offset in the coordinates for the curvature calculation, and the spacing is adjusted for the diameter of the head by 2.50 mm. The uncertainty of the head diameter adjustment is unknown, but the test results presented list a range from 2.4 to 2.9 mm. Based on that data, a 9.5% uncertainty is assigned to the head adjustment. The 9.5% adjustment includes the initial ±0.05 mm spacing uncertainty.

Finally, the LVDT is a long slender structure and there is some lateral movement of the probe stem that has been identified through testing. At 5 Hz the stem flexure was estimated as producing an ~18% bias in the curvature, and for this reason curvatures and gauge strains are reduced by 18% (in addition to the spacing correction). It is expected that there should be some directional difference in this value. That is, when the specimen is moving towards the LVDT bank, the bias is likely different than when the specimen is moving away from the LVDT bank. The expected directional difference is not currently reflected in the data processing. The 18% reduction was evaluated using strain gauged polycarbonate rod specimens. Given the difference in specimen surface conditions (affecting drag on the LVDT) and without a deep dive into the strain gauge response, the 18% is assigned an uncertainty of ±50% for the purpose of this study. The equivalent adjustment of h to achieve the 18% reduction in curvature is an 11% increase in spacing, from 12 to 13.3 mm, and the 50% uncertainty on the 18% in curvature is an additional equivalent h adjustment of 0.75 mm. Therefore, for purposes of this study, h is assigned as 13.3 mm ± 2.50(0.095) + 0.75 mm = 0.0133 m ± 0.001 m.

G-3.2.3 Estimated combined curvature uncertainty

Using the approach described in Eq. G-1, Eqs. G-2 though G-5, the individual uncertainty terms detailed in Subsections G-3.1.1 and G-3.1.2, and the MATLAB Symbolic Toolbox, the combined uncertainty of the curvature (in m^{-1}) is evaluated as follows:

$$\sqrt{\begin{array}{l} \dfrac{1.089e-11\left(2.0\left(d_2+\frac{\sigma_{16}}{\sigma_{17}}\right)\sigma_3+\frac{2.0\,\sigma_8\,(d_1-1.0\,d_2)\,\sigma_3}{h}\right)^2}{\sigma_1}+ \\[3ex] \dfrac{1.089e-11\left(2.0\,(\sigma_6+\sigma_7)\left(d_2+\frac{\sigma_{16}}{\sigma_{17}}\right)+2.0\,\sigma_8\left(\frac{\sigma_{13}}{h}+\frac{(d_1-1.0\,d_2)\,(\sigma_6+\sigma_7+0.5)}{h}\right)\right)^2}{\sigma_1}+ \\[3ex] \dfrac{1.089e-11\left(2.0\left(\frac{\sigma_{13}}{h}+\frac{(d_1-1.0\,d_2)\,(\sigma_4+\sigma_5-0.5)}{h}\right)\sigma_8+2.0\left(d_2+\frac{\sigma_{16}}{\sigma_{17}}\right)(\sigma_4+\sigma_5-1.0)\right)^2}{\sigma_1}+ \\[3ex] \dfrac{2.5e-7\left(2.0\left(d_2+\frac{\sigma_{16}}{\sigma_{17}}\right)\sigma_2+2.0\,\sigma_8\left(\frac{(d_1-1.0\,d_2)\,\sigma_2}{h}-\frac{1.0\,(d_1-1.0\,d_2)\,\sigma_{13}}{h^2}+0.5\right)\right)^2}{\sigma_1} \end{array}}, \qquad \text{(G-1)}$$

where

$$\sigma_1=\left(\sigma_8{}^2+\left(d_2+\frac{\sigma_{16}}{\sigma_{17}}\right)^2\right)^3, \qquad \text{(G-2)}$$

$$\sigma_2=\frac{\frac{d_1+d_2}{d_2-1.0\,d_3}-\frac{1.0\,(d_2+d_3)}{d_1-1.0\,d_2}+\frac{6.0\,h^2}{\sigma_{18}}}{\sigma_{17}}- $$
$$\frac{1.0\left(\frac{2.0}{d_1-1.0\,d_2}-\frac{2.0}{d_2-1.0\,d_3}\right)\sigma_{16}}{\sigma_{17}{}^2}, \qquad \text{(G-3)}$$

$$\sigma_3=\frac{\sigma_{10}-\frac{1.0\,h}{d_1-1.0\,d_2}+\sigma_9}{\sigma_{17}}+\frac{2.0\,h\,\sigma_{16}}{\sigma_{17}{}^2\,\sigma_{14}}, \qquad \text{(G-4)}$$

$$\sigma_4=\frac{\frac{h}{d_1-1.0\,d_2}-\frac{1.0\,h}{d_2-1.0\,d_3}+\sigma_{10}+\sigma_{12}+\sigma_9-\sigma_{11}}{\sigma_{17}}, \qquad \text{(G-5)}$$

$$\sigma_5=\frac{\left(\frac{2.0\,h}{\sigma_{15}}+\frac{2.0\,h}{\sigma_{14}}\right)\sigma_{16}}{\sigma_{17}{}^2}, \qquad \text{(G-6)}$$

$$\sigma_6 = \frac{\frac{h}{d_2 - 1.0\,d_3} + \sigma_{12} - \sigma_{11}}{\sigma_{17}}, \tag{G-7}$$

$$\sigma_7 = \frac{2.0\,h\,\sigma_{16}}{\sigma_{17}^2\,\sigma_{15}}, \tag{G-8}$$

$$\sigma_8 = 0.5\,h + \frac{(d_1 - 1.0\,d_2)\,\sigma_{13}}{h}, \tag{G-9}$$

$$\sigma_9 = \frac{2.0\,h^3}{(d_1 - 1.0\,d_2)\,\sigma_{14}}, \tag{G-10}$$

$$\sigma_{10} = \frac{h\,(d_1 + d_2)}{\sigma_{14}}, \tag{G-11}$$

$$\sigma_{11} = \frac{2.0\,h^3}{\sigma_{15}\,(d_2 - 1.0\,d_3)}, \tag{G-12}$$

$$\sigma_{12} = \frac{h\,(d_2 + d_3)}{\sigma_{15}}, \tag{G-13}$$

$$\sigma_{13} = 0.5\,d_1 + 0.5\,d_2 + \frac{\sigma_{16}}{\sigma_{17}}, \tag{G-14}$$

$$\sigma_{14} = (d_2 - 1.0\,d_3)^2, \tag{G-15}$$

$$\sigma_{15} = (d_1 - 1.0\,d_2)^2, \tag{G-16}$$

$$\sigma_{16} = \frac{h\,(d_1 + d_2)}{d_2 - 1.0\,d_3} - \frac{1.0\,h\,(d_2 + d_3)}{d_1 - 1.0\,d_2} + \frac{2.0\,h^3}{\sigma_{18}}, \tag{G-17}$$

$$\sigma_{17} = \frac{2.0\,h}{d_1 - 1.0\,d_2} - \frac{2.0\,h}{d_2 - 1.0\,d_3}, \text{ and} \tag{G-18}$$

$$\sigma_{18} = (d_1 - 1.0\,d_2)\,(d_2 - 1.0\,d_3). \tag{G-19}$$

The typical range of a test (d_1, d_2, d_3 ~0.05 to 0.08 mm) yields a radius of approximately 8.85 m. The curvature is highly dependent on the magnitude of the differential between d_2 and d_1/d_3. Using a small differential within the typical range (e.g., $d_1 = 0.00005$, $d_2 = 0.000052$, $d_3 = 0.0000502$ m), the radius is 44.4 m, the curvature is 0.022 m^{-1}, and the curvature uncertainty is $\pm$ 0.092 m^{-1}. Using a large differential within the range (e.g., $d_1 = 0.00005$, $d_2 = 0.00008$, $d_3 = 0.0000502$ m) the radius is 3.0 m, the curvature is 0.339 m^{-1}, and the curvature uncertainty is $\pm$ 0.105 m^{-1}. Thus, very low differentials (bending moments <7 N-m applied in the test or a specimen having a large rigidity) result in larger relative uncertainty. It is notable that the tests reporting a very low curvature generally also had a very high reported rigidity. It is not clear whether the low curvature is a consequence of the high rigidity, or vice versa. Fig. G-2 provides the uncertainty

estimate in a graphical format. The polynomial curve fit can be used to estimate the uncertainty of sister rod measurements and previous measurements.
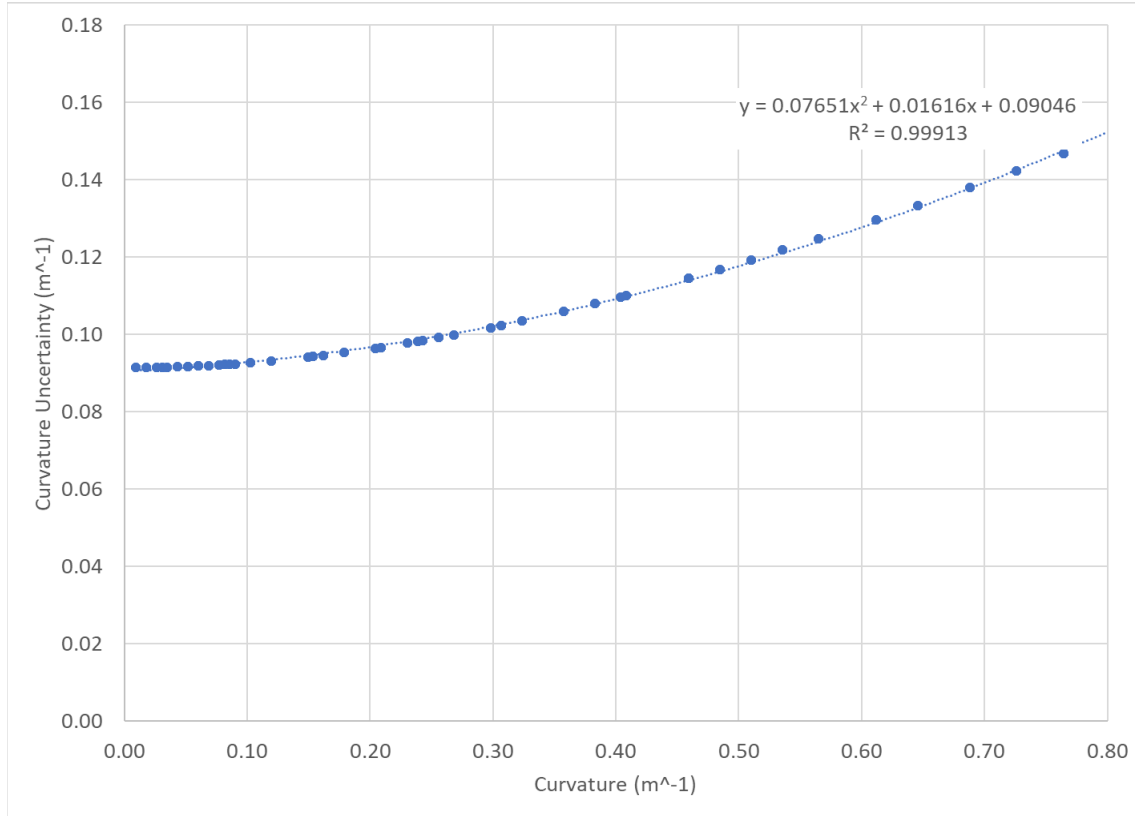

Figure G-2 Curvature uncertainty estimate as a function of curvature measurement.

G-3.3 Bending Moment Uncertainty

The average moment applied to the rod is:

$$M = F \times L \tag{G-25}$$

where F is the averaged value of the load applied at the time span of interest by the CIRFT motors and L is the fixed U-frame loading arm length (101.60 ± 0.05 mm).

Using the approach described in Eq. G-1 and the moment equation (Eq. G-6), the combined uncertainty of the bending moment is:

$$M_{uncertainty} = \sqrt{79.14\ L^2 + (2.5E - 11)\ F^2}\ \ in\ N - m \tag{G-26}$$

The typical range of force measured is on the order of 50 to 350 N and the associated typical measured moment and uncertainty is in the range of 5 ± 0.8 N-m to 35.5 ± 0.8 N-m. The uncertainty is relatively fixed and is almost entirely related to the length of the loading arm and its uncertainty.

G-3.4 Strain Uncertainty

The maximum gauge strain, which occurs at the maximum deflections in the cycle and at the outermost radius of the rod, is calculated as the curvature multiplied by the distance to the neutral axis:

$$\varepsilon = \kappa \times y_{max}. \qquad (G\text{-}27)$$

y_{max}, the distance to the neutral axis, is the radius of the rod and is nominally assumed as 4.75 mm; it is not assigned an uncertainty because it is not measured in this test. Thus, the uncertainty related to the strain is the uncertainty of the curvature measurement multiplied by y_{max}.

The typical strain magnitude and uncertainty ranges from $0.03 \pm 0.044\%$ to $0.30 \pm 0.063\%$. In other words, given a test with a measured curvature at the lower end of the strain range (e.g., at a nominal strain of 0.03%), the uncertainty term results in the information that the real strain lies somewhere in the range between -0.014% and 0.074%. At the upper end of the test range, where the nominal strain is 0.30%, the strain with the uncertainty applied is between 0.237% and 0.363%. Fig. G-3 provides the strain uncertainty estimate in a graphical format. The polynomial curve fit can be used to estimate the uncertainty of sister rod measurements and previous measurements. The number of cycles to failure versus strain amplitude is shown in Fig. G-4 with the calculated uncertainty applied to the sister rod measurements.

The plotted data follows a fitted curve with equation $y = 0.161082x^2 + 0.016156x + 0.042968$, $R^2 = 0.999130$. The vertical axis is Strain Uncertainty (%) ranging from 0.0000 to 0.0800, and the horizontal axis is Strain (%) ranging from 0.00 to 0.45.
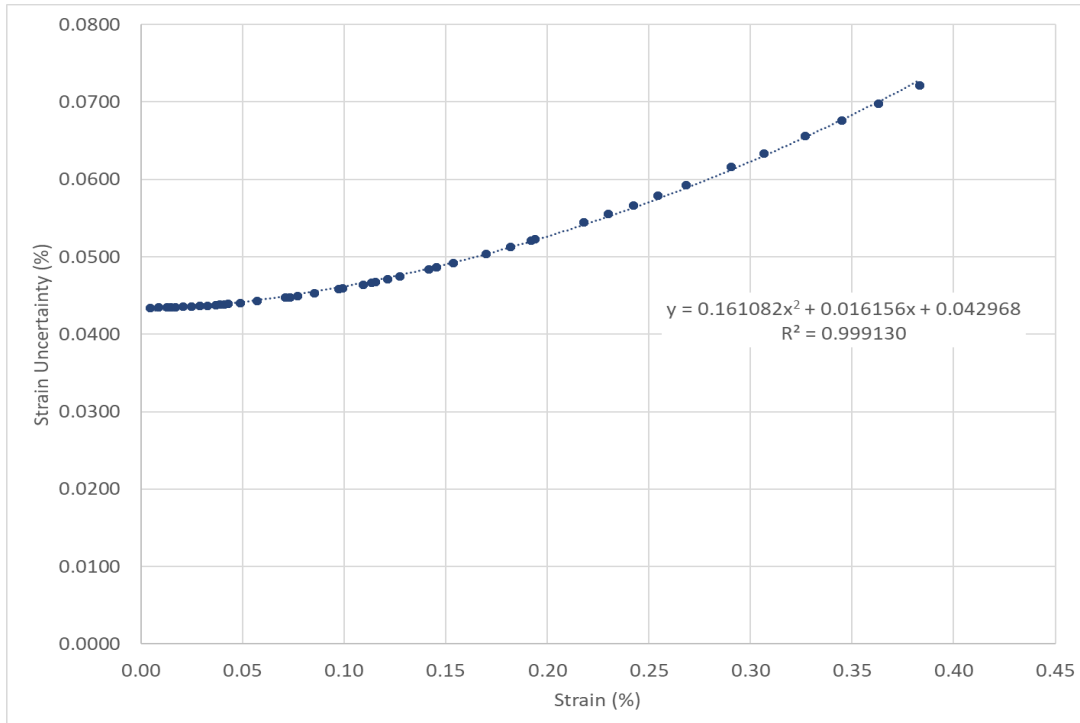
Figure G-3. Estimated strain uncertainty as a function of calculated strain.
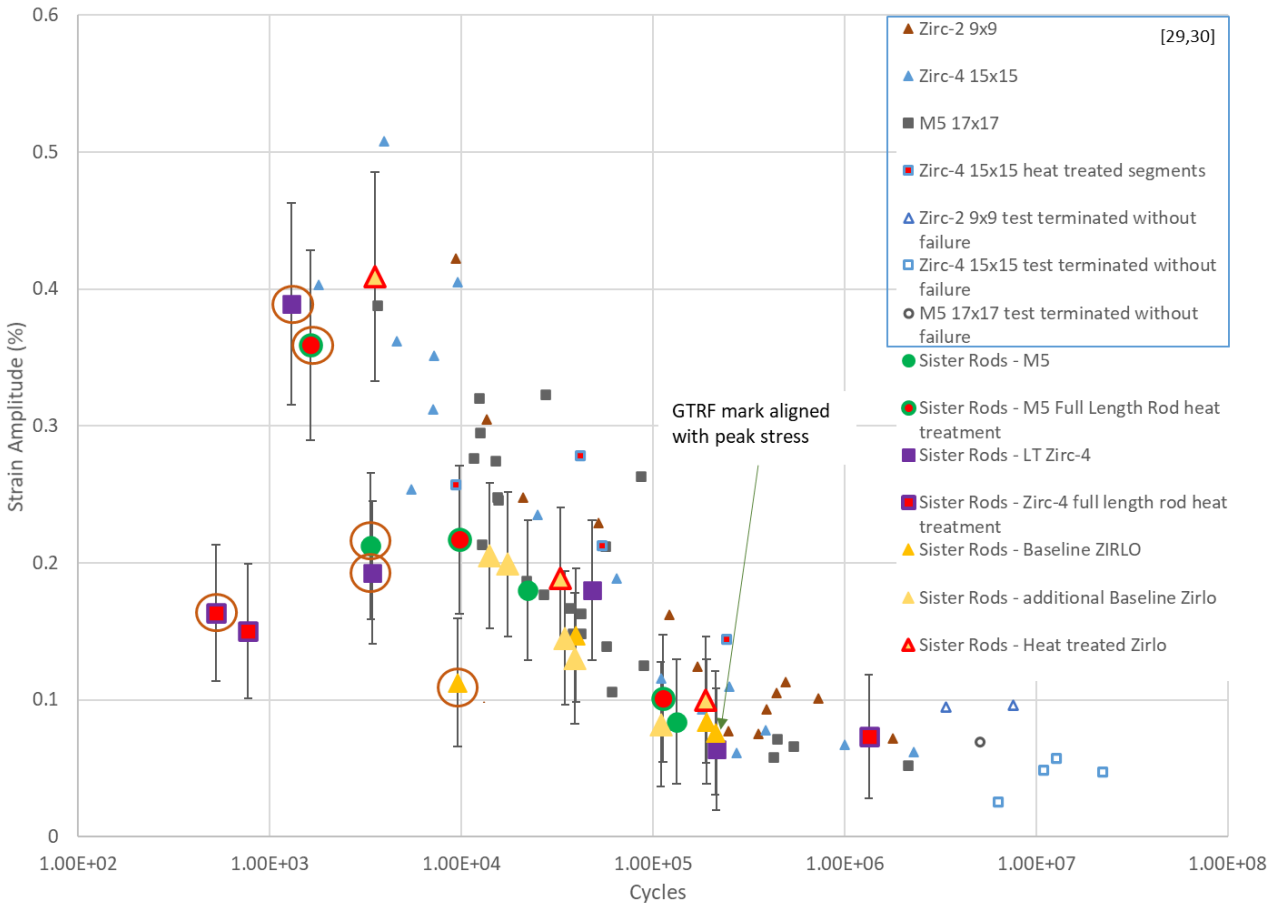
Figure G-4. Sister rod strain amplitude with uncertainty shown and reference data.

G-3.5 Stress Uncertainty

The maximum rod stress is calculated as:

$$\sigma = M \times y_{max} / I \tag{G-28}$$

where I is the area moment of inertia of the composite SNF rod calculated based on the geometry of cladding and solid pellet section. Similar to y_{max}, I is assigned a nominal value based on the assumed cross-sectional geometry of the rod and does not have a measurement uncertainty assigned. Thus, the uncertainty of the stress is relatively fixed as dominated by the uncertainty of the moment multiplied by (y_{max}/I), 10.65 MPa.

The typical order of magnitude is 20 to 200 ± 11 MPa. The number of cycles to failure versus stress amplitude is shown in Fig. G-5 with the calculated uncertainty applied to the sister rod measurements.
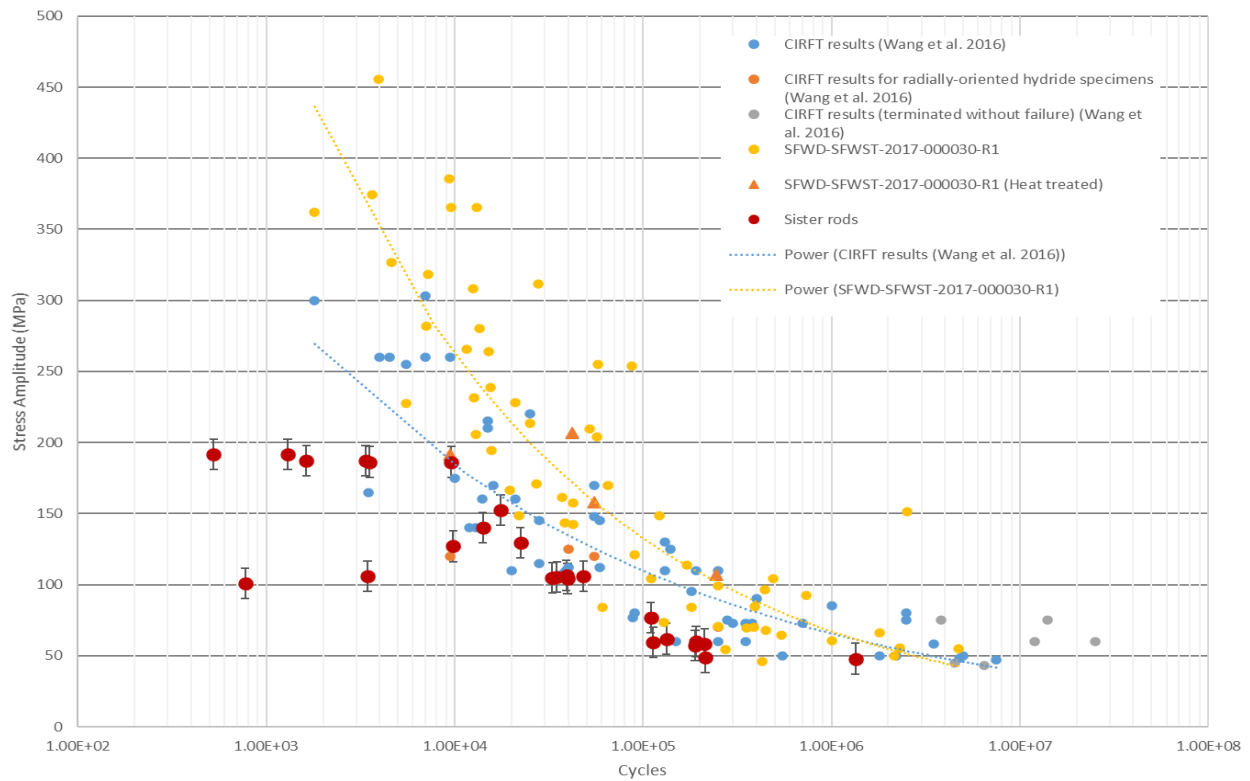
Figure G-5. Sister rod stress amplitude with uncertainty shown and reference data

G-3.6 Flexural Rigidity Uncertainty

The flexural rigidity, *EI*, provides a means to generate the stress-strain relationship associated with M-κ. The average calculated bending moment (ΔM) and average measured curvature ($\Delta \kappa$) are used to characterize the average flexural rigidity over the timespan of interest:

$$EI = \Delta M / \Delta \kappa. \tag{G-29}$$

Using the approach described in Eq. (G-1) and the flexural rigidity equation above, the combined uncertainty of the flexural rigidity is

$$
\left[79.14\, L^2\, \sigma_1 + 2.5e-11\, \text{load}^2\, \sigma_1 + \frac{1.089e-11\, L^2\, \text{load}^2 \left(2.0 \left(d_2 + \frac{\sigma_{16}}{\sigma_{17}} \right) \sigma_3 + \frac{2.0\, \sigma_8\, (d_1 - 1.0\, d_2)\, \sigma_3}{h} \right)^2}{\sigma_1} \right.
$$

$$
+ \frac{1.089e-11\, L^2\, \text{load}^2 \left(2.0\, (\sigma_6 + \sigma_7) \left(d_2 + \frac{\sigma_{16}}{\sigma_{17}} \right) + 2.0\, \sigma_8 \left(\frac{\sigma_{13}}{h} + \frac{(d_1 - 1.0\, d_2)(\sigma_6 + \sigma_7 + 0.5)}{h} \right) \right)^2}{\sigma_1}
$$

$$
+ \frac{1.089e-11\, L^2\, \text{load}^2 \left(2.0 \left(\frac{\sigma_{13}}{h} + \frac{(d_1 - 1.0\, d_2)(\sigma_4 + \sigma_5 - 0.5)}{h} \right) \sigma_8 + 2.0 \left(d_2 + \frac{\sigma_{16}}{\sigma_{17}} \right) (\sigma_4 + \sigma_5 - 1.0) \right)^2}{\sigma_1} \tag{G-20}
$$

$$
\left. + \frac{2.5e-7\, L^2\, \text{load}^2 \left(2.0 \left(d_2 + \frac{\sigma_{16}}{\sigma_{17}} \right) \sigma_2 + 2.0\, \sigma_8 \left(\frac{(d_1 - 1.0\, d_2)\, \sigma_2}{h} - \frac{1.0\, (d_1 - 1.0\, d_2)\, \sigma_{13}}{h^2} + 0.5 \right) \right)^2}{\sigma_1} \right]^{1/2}
$$

where

$$\sigma_1 = \sigma_8{}^2 + \left(d_2 + \frac{\sigma_{16}}{\sigma_{17}} \right)^2, \tag{G-21}$$

$$\sigma_2 = \frac{\frac{d_1 + d_2}{d_2 - 1.0\, d_3} - \frac{1.0\,(d_2 + d_3)}{d_1 - 1.0\, d_2} + \frac{6.0\, h^2}{\sigma_{18}}}{\sigma_{17}} - \frac{1.0 \left(\frac{2.0}{d_1 - 1.0\, d_2} - \frac{2.0}{d_2 - 1.0\, d_3} \right) \sigma_{16}}{\sigma_{17}{}^2}, \tag{G-22}$$

$$\sigma_3 = \frac{\sigma_{10} - \frac{1.0\, h}{d_1 - 1.0\, d_2} + \sigma_9}{\sigma_{17}} + \frac{2.0\, h\, \sigma_{16}}{\sigma_{17}{}^2\, \sigma_{14}}, \tag{G-23}$$

$$\sigma_4 = \frac{\frac{h}{d_1 - 1.0\, d_2} - \frac{1.0\, h}{d_2 - 1.0\, d_3} + \sigma_{10} + \sigma_{12} + \sigma_9 - \sigma_{11}}{\sigma_{17}}, \tag{G-24}$$

$$\sigma_5 = \frac{\left(\frac{2.0\, h}{\sigma_{15}} + \frac{2.0\, h}{\sigma_{14}} \right) \sigma_{16}}{\sigma_{17}{}^2}, \tag{G-25}$$

$$\sigma_6 = \frac{\frac{h}{d_2 - 1.0\, d_3} + \sigma_{12} - \sigma_{11}}{\sigma_{17}}, \tag{G-26}$$

$$\sigma_7 = \frac{2.0 \, h \, \sigma_{16}}{\sigma_{17}^2 \, \sigma_{15}}, \tag{G-27}$$

$$\sigma_8 = 0.5 \, h + \frac{(d_1 - 1.0 \, d_2) \, \sigma_{13}}{h}, \tag{G-28}$$

$$\sigma_9 = \frac{2.0 \, h^3}{(d_1 - 1.0 \, d_2) \, \sigma_{14}}, \tag{G-29}$$

$$\sigma_{10} = \frac{h \, (d_1 + d_2)}{\sigma_{14}}, \tag{G-30}$$

$$\sigma_{11} = \frac{2.0 \, h^3}{\sigma_{15} \, (d_2 - 1.0 \, d_3)}, \tag{G-31}$$

$$\sigma_{12} = \frac{h \, (d_2 + d_3)}{\sigma_{15}}, \tag{G-32}$$

$$\sigma_{13} = 0.5 \, d_1 + 0.5 \, d_2 + \frac{\sigma_{16}}{\sigma_{17}}, \tag{G-33}$$

$$\sigma_{14} = (d_2 - 1.0 \, d_3)^2, \tag{G-34}$$

$$\sigma_{15} = (d_1 - 1.0 \, d_2)^2, \tag{G-35}$$

$$\sigma_{16} = \frac{h \, (d_1 + d_2)}{d_2 - 1.0 \, d_3} - \frac{1.0 \, h \, (d_2 + d_3)}{d_1 - 1.0 \, d_2} + \frac{2.0 \, h^3}{\sigma_{18}}, \tag{G-36}$$

$$\sigma_{17} = \frac{2.0 \, h}{d_1 - 1.0 \, d_2} - \frac{2.0 \, h}{d_2 - 1.0 \, d_3}, \text{ and} \tag{G-37}$$

$$\sigma_{18} = (d_1 - 1.0 \, d_2) \, (d_2 - 1.0 \, d_3). \tag{G-38}$$

The uncertainty in the flexural rigidity is greatly influenced by the uncertainty in the curvature. Low curvatures have a high rigidity uncertainty that is generally 5 to 20 times the uncertainty at higher curvatures. The EI uncertainty is also sensitive to the load cell uncertainty, but to a much lesser degree than the curvature uncertainty. Within the range of the experiment's applied moments, the flexural rigidity ranges from 100 ± 170 (low curvature) to 11 ± 3 N-m^2 (high curvature).

Figure G-6 provides the rigidity uncertainty estimate as a function of the calculated rigidity. In this graphical format, it is easy to see the effect the moment has on the rigidity and its associated measurement uncertainty. The most dominant parameter, the LVDT measurement uncertainty, is illustrated in Figure G-7, where the differential between the center LVDT measurement and the side LVDT measurements is plotted with the overall flexural rigidity uncertainty. As the difference between the LVDT increases (implying larger curvatures), the LVDT measurement uncertainty is less significant, and the rigidity uncertainty is decreased. To apply the estimated flexural rigidity within the sister rod data and past data, the moment is first determined. The uncertainty is interpolated using the polynomial curve fits for the nearest moments. The

specimen burnup versus flexural rigidity is shown in Figure G-8, with the calculated uncertainty applied to the sister rod measurements.
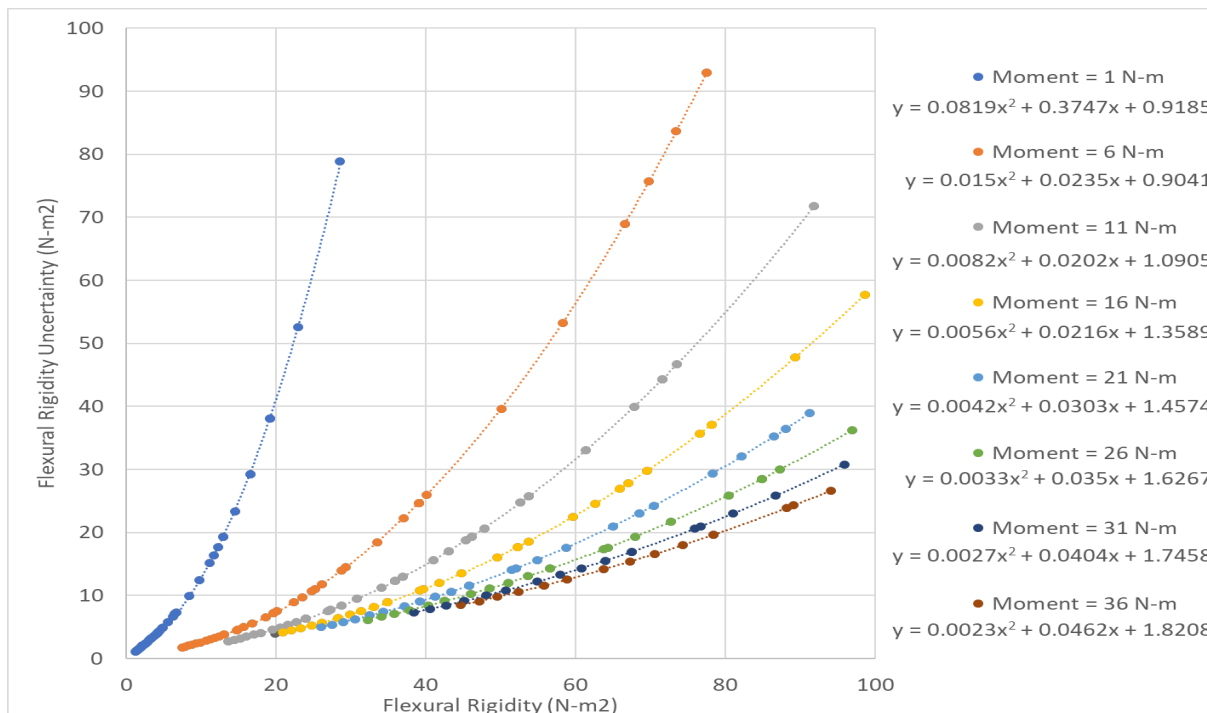

Figure G-6. Estimated flexural rigidity uncertainty as a function of calculated flexural rigidity.
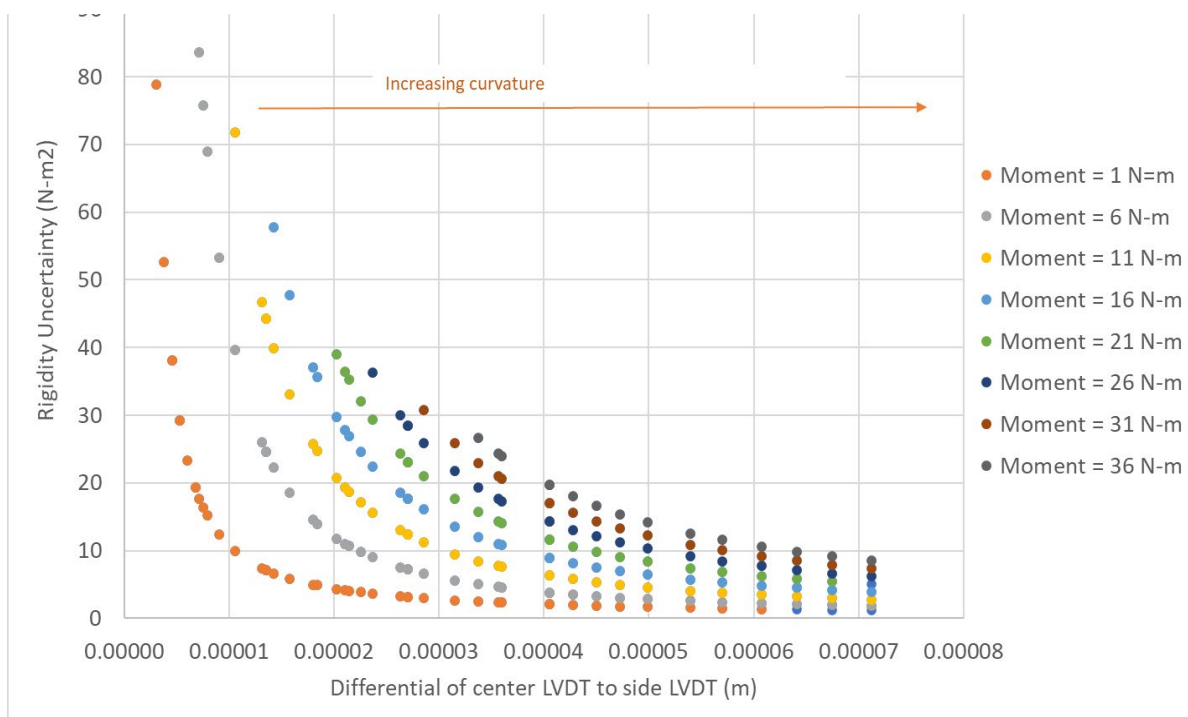

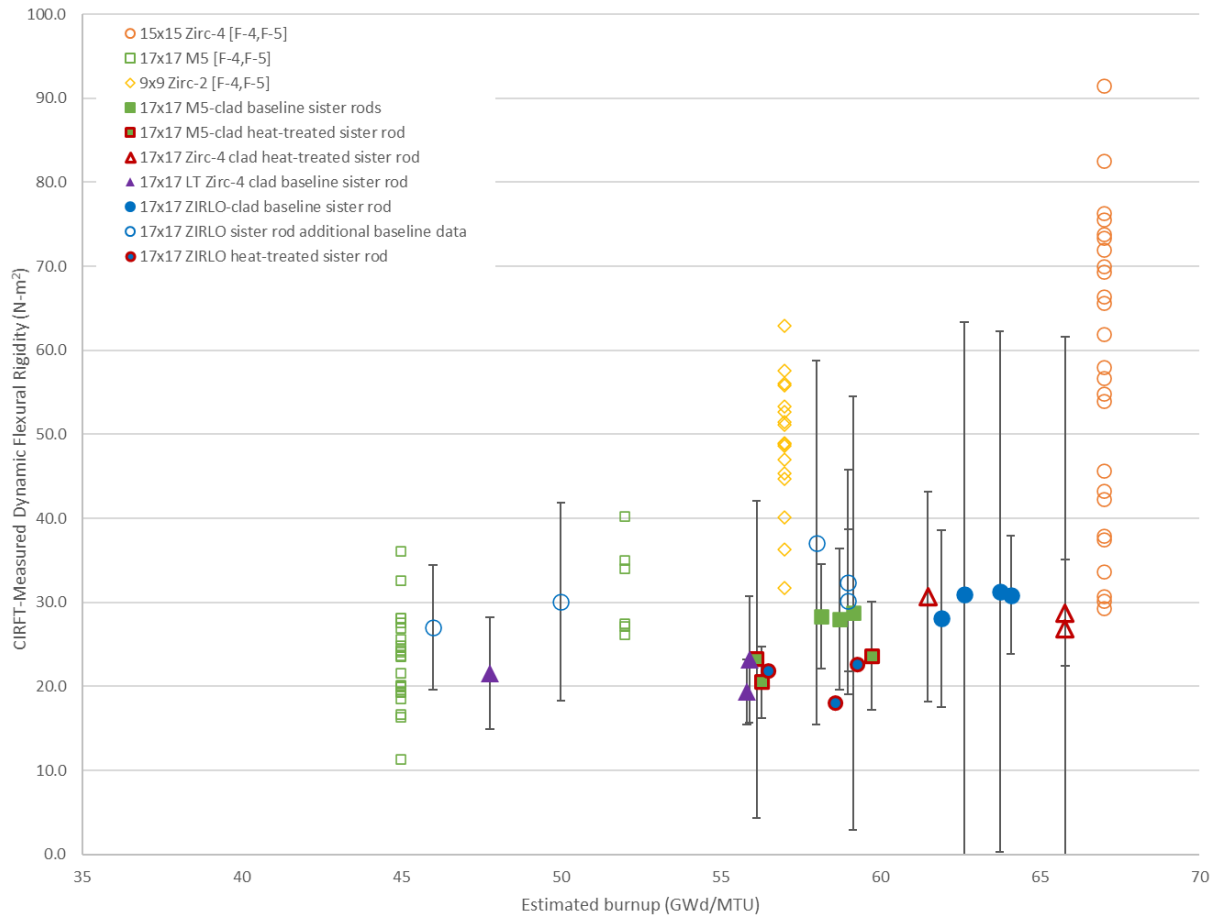**Figure G-7. Effect of LVDT differential on rigidity uncertainty.**

Figure G-8. Sister rod CIRFT-measured flexural rigidity with uncertainty shown and reference data.

G-4. Summary

The uncertainty associated with each of the CIRFT primary and secondary parameters is summarized in Table G-1.

Table G-1. Summary of Uncertainty terms for CIRFT Parameters.

Parameter	Measurement range	Uncertainty
Cycles to failure	N/A	Unknown but estimated to be small
Curvature, m^{-1}	0 to 0.80	$0.07651\ K^2 + 0.01616K + 0.09046$
Bending moment, N-m	0 to 40	~0.8
Strain, %	0 to 0.45	$0.161082\ \varepsilon^2 + 0.016156\ \varepsilon + 0.042968$
Stress, MPa	0 to 450	~11
Flexural rigidity, N-m^2	0 to 100	
	For moment = 1 N-m	$0.0819\ EI^2 + 0.3747\ EI + 0.9185$
	For moment = 6 N-m	$0.015\ EI^2 + 0.0235\ EI + 0.9041$
	For moment = 11 N-m	$0.0082\ EI^2 + 0.0202\ EI + 1.0905$
	For moment = 16 N-m	$0.0056\ EI^2 + 0.0216\ EI + 1.3589$
	For moment = 21 N-m	$0.0042\ EI^2 + 0.0303\ EI + 1.4574$
	For moment = 26 N-m	$0.0033\ EI^2 + 0.035\ EI + 1.6267$
	For moment = 31 N-m	$0.0027\ EI^2 + 0.0404\ EI + 1.7458$
	For moment = 36 N-m	$0.0023\ EI^2 + 0.0462\ EI + 1.8208$

REFERENCES

[G-1.] J.-A. Wang and H. Wang, *FY 2017 Status Report: CIRFT Data Update and Data Analyses for Spent Nuclear Fuel Vibration Reliability Study, Revision 1*, ORNL/SPR-2017/521, SFWD-SFWST-2017-000030/R1 (2017).

[G-2.] J.-A. Wang and H. Wang, *Mechanical Fatigue Testing of High Burnup Fuel for Transportation Applications,* NUREG/CR-7198/R1 (2017).